

ANSYS-CFX Simulation and Experimental Studies on Centrifugal Pump Impeller Design: Performance Effects Using Corrosive and Non-corrosive Resources

Isa Umaru Usman¹, Kashif Abbas², Abdulhalim Musa Abubakar^{1,3}, Ronny Mönnig⁴, Aminullah Zakariyyah Abdul^{1,5}, Mazen Abdul-Jabbar Alhodali⁶

¹Department of Chemical Engineering, Faculty of Engineering, University of Maiduguri (UNIMAID), P.M.B. 1069, Bama Road, Maiduguri, Borno State, Nigeria

²School of Mechanical Engineering, Faculty of Engineering, Xian Jiaotong University, Shaanxi, China

³Department of Chemical Engineering, Faculty of Engineering, Modibbo Adama University (MAU), P.M.B. 2076, Yola, Adamawa State, Nigeria

⁴Project Manager: Department of System Calibration | Business Area Future Powertrain, IAV, GmbH, Berlin, Germany

⁵Department of Chemical Engineering, Faculty of Engineering, Federal University Wukari, Wukari, Taraba State, Nigeria

⁶YemenLNG Company, Yemen

Article Info

Article history:

Received Mar 2, 2023

Revised Mar 26, 2023

Accepted Apr 11, 2023

Keywords:

ANSYS

Centrifugal pump

Impeller

Computational fluid dynamics

Performance curve

ABSTRACT

Corrosive fluids, namely saline water, hydrochloric acid and methanol and non-corrosive fluids, namely, water, gasoline and kerosene can be tested for efficiency and reliability on an existing H47 centrifugal pump impeller's performance. To analyze the pump performance, ANSYS student version 2022 software was used – wherein; head rise (H), pump speed (N), discharge rate (Q) and inlet pressure of 20-120m, 2000rpm, 144m³/h and 0 atm were respectively specified as initial and boundary conditions in the computational fluid dynamics (CFD) tool. CFD for inlet and exit blade angles of 35°, 38°, 41° and 47°, 50°, 53° were respectively simulated for all fluid type using a 7-bladed impeller to obtain contour plots and pressure and velocity distribution results of the analysis. It was deduced that the overall efficiency of the centrifugal pump depends on the outlet blade angle and fluid type, while the power used rises with both inlet and outlet blade angles. Further studies should be channeled towards analyzing the variations in N, Q, H, impeller blade number (Z) and its width, for this particular type of impeller.

This is an open access article under the [CC BY](#) license.



Corresponding Author:

Abdulhalim Musa Abubakar,
Department of Chemical Engineering,
Modibbo Adama University,
Yola, Adamawa State, Nigeria.
Email: abdulhalim@mau.edu.ng

1. INTRODUCTION

A centrifugal pump is a form of turbo machine in which fluid centrifugal force converts mechanical energy into pressure energy. The pump's two principal parts are the diffuser and the impeller. A centrifugal pump's impeller is a rotating part that accelerates the fluid away from the center of rotation to transfer energy from the pump's motor to the fluid being pushed. Prasad et al. (2013), in their work, suggested Inconel alloy 740 as the best material for impeller design apart from others it is frequently made from; such as cast iron, steel, bronze, brass, aluminum, or plastic, which are either corrodible and non-corrodible materials. They find

applications in many industrial settings, namely water, sewage, drainage and chemical industries. Fluids pumped using impellers might be corrosive, non-corrosive and/or viscous in nature. The velocity of the impeller is converted to pressure when the pump casing restricts the fluid's outward flow. The diffuser, often referred to as the volute, which houses the impeller also collects and directs fluids off the impeller. As the fluid moves through the impeller, which is spinning quickly, it gains momentum. Via specifically designed tunnels, the diffuser absorbs the fluid's velocity and transforms it to pressure before routing the flow to the pump's outlet or to the next. The pressure that a pump produce is influenced by the impeller diameter, the number of blades, the size of the impeller eye, and the shaft speed. The capacity is determined by the impeller's exit width, but as for the inlet width, a detailed explanation was given by Zhang et al. (2014) which is one of the limitation of this work. The head and capacity of the motor are the main factors that determine its horsepower size. Energy usage increases as the amount of fluid that needs to be pumped increases.

The pump produces the same head of liquid regardless of the density of the fluid being pumped. The exact geometries of the impeller and casing hydraulic channels are very important in order to obtain the maximum efficiency, which is often between 65-70%. Centrifugal pump performance curves are commonly illustrated with head produced on the vertical axis and flow on the horizontal axis. Given the amount of electricity pumping systems consume, even small improvements in pumping efficiency could result in significant electrical cost savings. One of the least effective parts of a pumping system is the pump, along with the motor, transmission drive, pipelines, and valves. A soft medium for predicting flow through pumps and the enhancement of their design is the Computational Fluid Dynamics (CFD), where parameters like blade number (Z), blade thickness, blade wrap angle and blade outlet angle in which its performance is dependent on are analyzed. Flow conditions are visualized in CFD simulations, whose outcome is used to predict or compute centrifugal pump performance to substitute or lessen the experiments in the development of pump design. Other merits are its reliability, cost and time savings, provision of precise and complete information about heating, ventilation, and air conditioning (HVAC) design parameters and performance prediction before amending and fitting the system. ANSYS-CFX is the most widely used CFD apparatus to study this performance. CFD uses fundamentally, numerical techniques to solve nonlinear differential equations describing fluid flow for predefined geometrics and boundary conditions – and in the process, it must satisfy conservation of mass, momentum and energy throughout the region in question. Simplifying assumptions (e.g., steady-state, in viscid, incompressible, two dimensional) are made to make the problem tractable to facilitate predictions for temperature, density, velocity and chemical concentrations for any region experiencing flow.

Previously, Chen et al. (2021) designed six impellers having varying blade inlet angles with ANSYS Bladegen and NX software. Han et al. (2018) investigates the effects of blade exit angles 24° , 26° and 28° and blade wrap angle on the optimized design of an impeller, where they found that the relative velocity in the pressure surface was much lesser than that of suction pressure. According to Yadav & Gahlot (2015), mixed flow pump impeller performance increases as outlet blade angle increases while inlet blade angle decreases in opposition to the outlet pressure which decreases. Furthermore, overall efficiency of the pump is proportional to the number of blades when ANSYS-CFX 14.0 software was used by the same author; a study that was carried out also by Susilo & Setiawan (2021). Bacharoudis et al. (2008) also observed that, as the outlet blade angle increases, the performance curve tends to be smoother and flatter for the whole range of flowrate specified. They further agreed to the fact that, at high flowrates, increase in the outlet blade angle will cause steady improvement in the hydraulic efficiency without having much effect on the head, as affirmed also by Ding et al. (2019) using similar software. Velocity and pressure distributions, shape of the impeller blades, effect of blade angle/profile on efficiency and power and how to reduce pressure fluctuations have all been studied previously without any regards to the fluid type. Thus, this study's goals are to evaluate the effectiveness of an existing centrifugal pump impeller, increase the effectiveness and dependability of a centrifugal pump impeller by altering the blade angle when using fluids of different properties, and conduct experimentation to evaluate the performance of a centrifugal pump impeller under pressure fluctuations using CFD. Because in the petroleum industry, to maximize the production rate of oil and gas, design of efficient centrifugal pump impeller plays a very critical role.

2. RESEARCH METHOD

2.1. Materials

A commercial ANSYS software student version 2022 was used on a Laptop PC, windows 10. Densities of corrosive and non-corrosive fluids used were sourced from the literature and shown in Table 1.

Table 1. Corrosive and Non-corrosive Fluids Used

S/No.	Fluids	Density (kg/m ³)
Corrosive		
1.	Saline Water	1031
2.	Hydrochloric acid	1169
3.	Methanol	792
Non-Corrosive		
4.	Water at 100°C	993
5.	Gasoline	720
6.	Kerosene	810

2.2. Methods

2.2.1. Experimental Setup and Specifications

H47 centrifugal pump type with head rise (H) of 20-120m, discharge rate (Q) of 144 m³/h and pump speed (N) of 2000 rpm was specified. Similar pump with different/unique feature was analyzed previously for performance by Adeniyi & Komolafe (2014). Table 2 shows the features of the specified centrifugal pump impeller.

Table 2. Features of the Centrifugal Pump Impeller

Dimensions	Measurements
Shaft diameter, D_s	40 mm
Eye diameter, D_o	124 mm
Hub diameter, D_h	106 mm
Inlet diameter, D_1	125 mm
Inlet blade width, b_1	54 mm
Outlet blade width, b_2	30 mm
Inlet blade angle, β_1	35°, 38°, 41°
Outlet blade angle, β_2	47°, 50°, 53°
Blade number, z	7
Blade thickness, t	16 mm
Outlet diameter, D_2	310 mm

2.2.2. Impeller Design for Efficiency Improvement

Finite element analysis (FEA), explicit and implicit methods, heat transport, structural analysis, and CFD are just a few of the analyses that were predicted using the engineering analysis tool employed for the study; i.e., ANSYS software [3]. In this study, the model construction and flow simulation were done in the ANSYS Workbench and ANSYS-CFX respectively as described by Rajendran & Purushothaman (2012). Vista Centrifugal Pump Design (CPD) in ANSYS software was used to construct the centrifugal pump impeller, which was then translated to the BladeGen. The designed blade was then examined in the AM design modeler after BladeGen data was transmitted to ANSYS Meshing (AM). The most suitable mesh for the analysis was automatically generated in AM utilizing the ANSYS Workbench CFX platform. Design Modeler was used to make the fillet. The mesh was moved to CFX, and CFX-Pre employed the Turbo wizard. In CFX-Solver, flow simulations were completed in 100 iterations, and all of the simulations converged in the same amount of repetition. As a result, the outcomes were seen in the CFD post (Turbo post). Final results were obtained in CFD post according to boundary conditions, giving precise analysis results. The results of pressure, density, and velocity are provided by the software calculator in the CFD post. The flow express is very important for performing CFD analysis which provided the results of fluids head, pressure, efficiency and pressure ratio explained in Muttali et al. (2014).

3. RESULTS AND DISCUSSIONS

3.1. ANSYS Software and Impeller Efficiency Calculations

It is one of the well-established and convenient analysis tools that has been successfully applied to solve engineering problems. As advance as it remains, the technology allows the calculation of the

simulations faster, more accurate and more efficient. Table 3 shows BladeGen calculated impeller data for the angles.

Table 3. Calculated Impeller Data from BladeGen for Various Angles

S/No.	Variables (m/s)	Definition	Impeller Inlet and Outlet Angles		
			35° – 47°	38° – 50°	41° – 53°
1.	C_{u1}	Inlet velocity of fluid	0.00	0.00	0.00
2.	C_{u2}	Outlet velocity of fluid	17.69	17.69	17.69
3.	W_1	Velocity of whirl of fluid	22.11	21.83	22.80
4.	W_2	Mean velocity of fluid at impeller hut outlet	16.35	16.06	16.90
5.	U_1	Tangential velocity of the impeller at the inlet	13.04	13.04	13.04
6.	U_2	Tangential velocity of the impeller at the outlet	32.42	32.42	32.42
7.	C_{m1}	Mean velocity of fluid at impeller hub inlet	17.85	17.51	18.71

Analytical calculations for the blade inlet angle of 35° and outlet angle of 47° for the efficiencies of the existing design of impeller were performed using Equations (1) and (2) respectively given Ding et al. (2019).

$$\text{Volumetric Efficiency} = \frac{1}{1+0.68(N)^{\frac{Z}{S}}} \quad (1)$$

$$\text{Hydraulic Efficiency} = \frac{\text{actual head of centrifugal pump}}{\text{total head of centrifugal pump}} \quad (2)$$

Where, blade number, $Z = 7$, suction side, $S = 143$, actual heat of the centrifugal pump = 50m and total head of centrifugal pump = 120m. This gives a volumetric efficiency of 69.72% and a hydraulic efficiency of 41.7%. Several other equations governing the centrifugal pump flow can be found in Adeniyi & Komolafe (2014).

3.2. Simulation Results

The impeller geometry was constructed in the ANSYS Workbench Vista CPD and the flow simulation was carried out using the ANSYS-CFX. To initialize and run the simulation, a hybrid initialization was used to obtain the results. The results of the simulations were in terms of pressure contour and vector velocity. After the analysis was carried out, the results were obtained from the software once the simulation has converged. For the flow simulation, various corrosive liquids (saline water, hydrochloric acid and methanol) and non-corrosive fluids (water, gasoline and kerosene) at 2000rpm rotating speeds were selected for different inlet and exit impeller angle of 35°, 38°, 41° and 47°, 50°, 53° respectively to be the variable factors in this project. The work did not however vary Z for the particular rotational speed chosen, as previously analyzed in Elyamin et al. (2019).

Results of the simulations were obtained from the CFD post software and compared among the three different inlet and outlet angle of impeller and the corrosive and non-corrosive working fluids earlier proposed by this author for the award of B.Eng. Degree in Chemical Engineering, in the University of Maiduguri, Nigeria [16, 17]. Input and output powers were calculated in order to obtain the impeller efficiency. The following results were taken in varying axis and cross sections, as would be seen in subsequent sub-headings.

3.2.1. Impeller Designed

Designed and meshed model for the simulations is depicted in Figures 1 and 2.

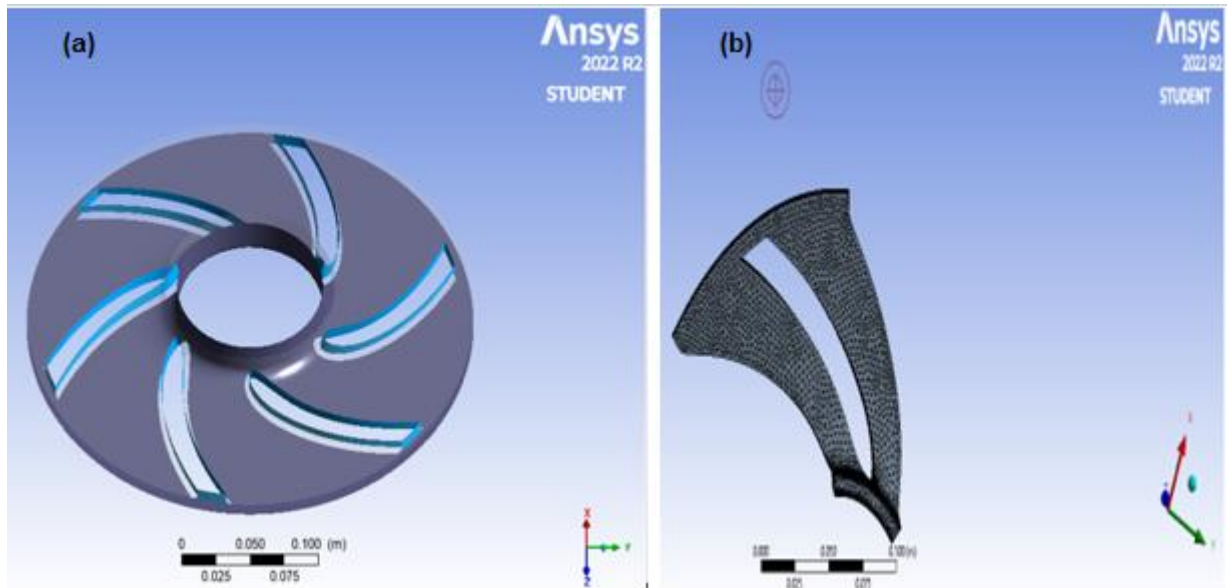


Figure 1: (a) The Designed Model and (b) The Meshed Model

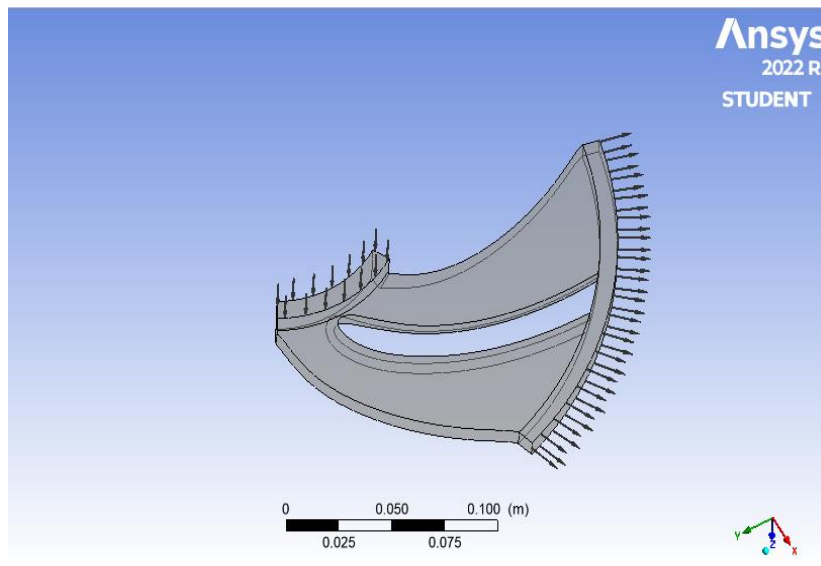


Figure 2: The Boundary Conditions

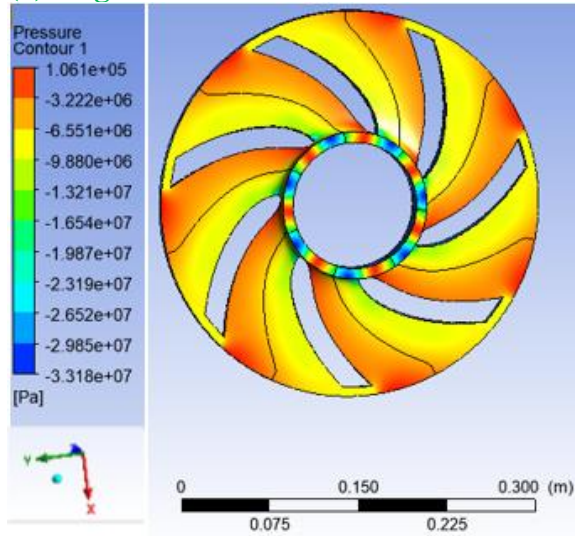
A pump impeller domain is considered as rotating frame of reference with a rotational speed of 2000 rpm. The boundary condition was inlet pressure of 0 atm, various mass flow of the selected fluids and 2000rpm. Working fluids in the pump are both the corrosive and non-corrosive fluids chosen. There are no slip wall conditions specified. The walls were assumed smooth and a steady state condition is considered.

Contour plots for the distributions of static pressure and velocity vector using ANSYS-CFX were also obtained, following steps followed by Murakami et al. (1980).

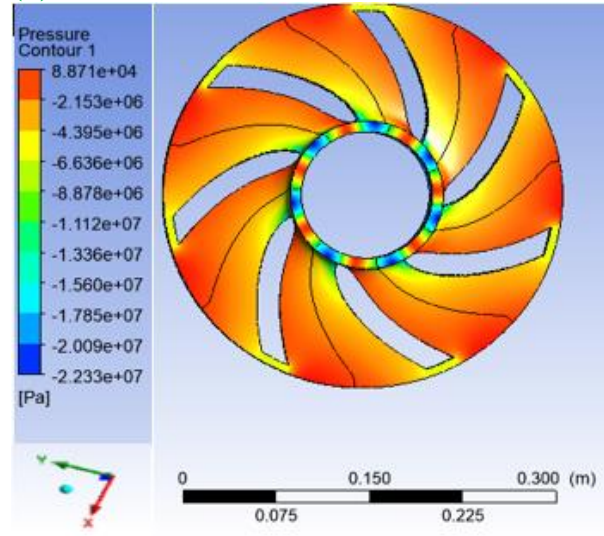
3.2.2. Pressure Distributions

Vivid explanations to pressure effect on the performance of the design are in Jia et al. (2018), which is similar to pressure distributions result trends found in this work. Figures 3, 4 and 5 represents the pressure distributions of the impeller across the specified angles for all fluid types. The pressure distributions of impeller across the impeller inlet angle of 35° and exit angle of 47° for various corrosive fluids are shown in Figure 3a. Pressure distribution across the impeller inlet angle of 38° and exit angle of 50° for various corrosive fluids (saline water, hydrochloric acid and methanol) have inlet pressure of -2233kPa, -1389kPa, -9807kPa and outlet pressure of 89kPa, 61kPa, 72kPa respectively, as illustrated in Figure 3b.

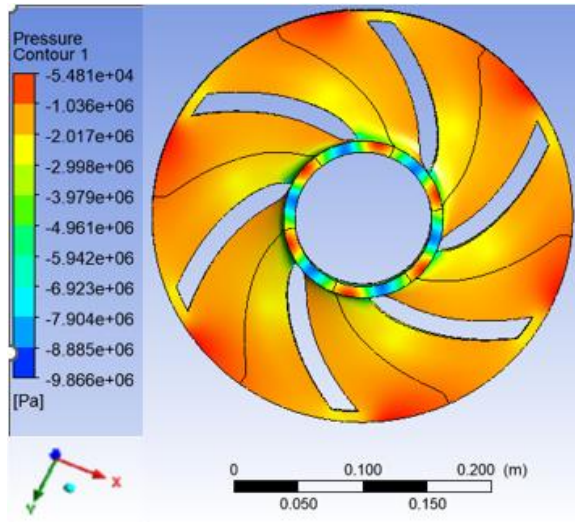
(a) Angle 35° and 47°



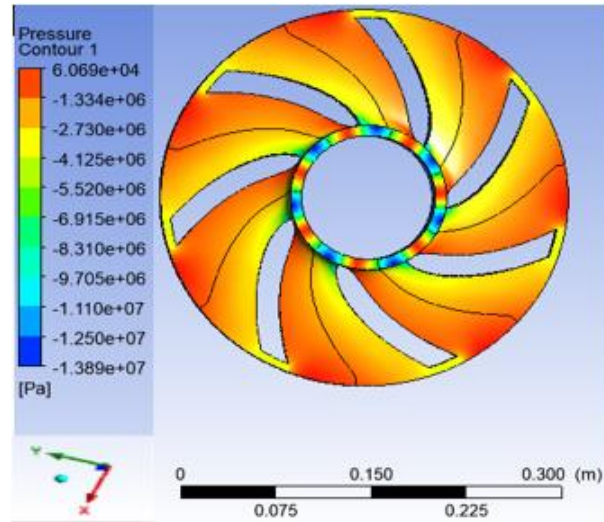
(b) 38° and 50°



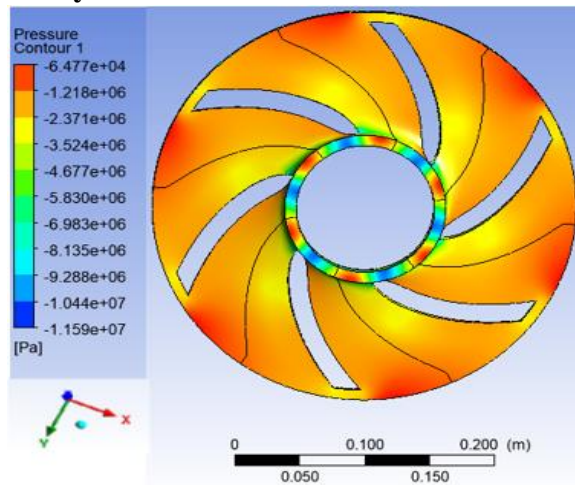
I. Saline Water



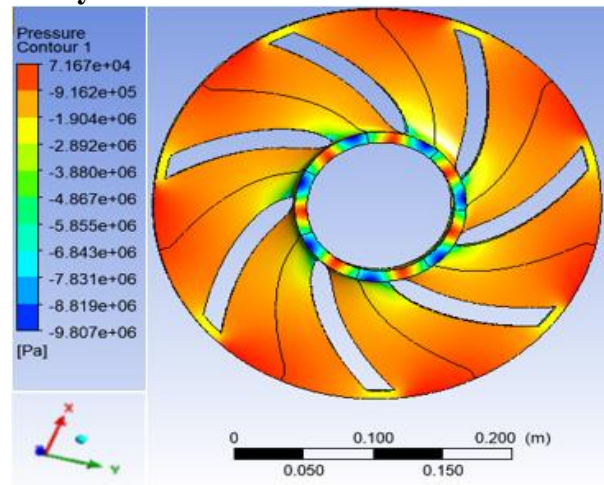
I. Saline Water



II. Hydrochloric Acid



II. Hydrochloric Acid

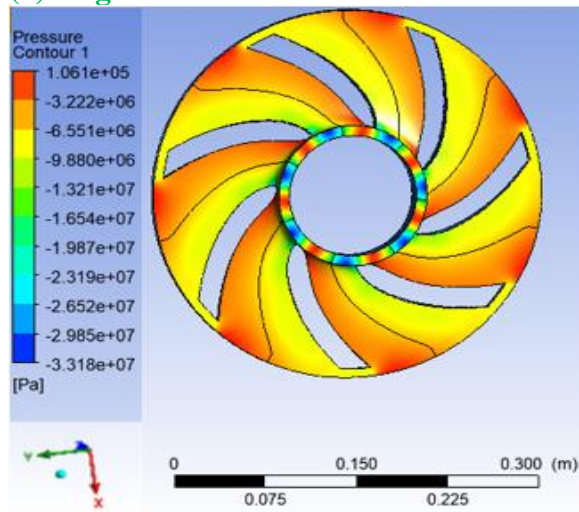


III. Methanol

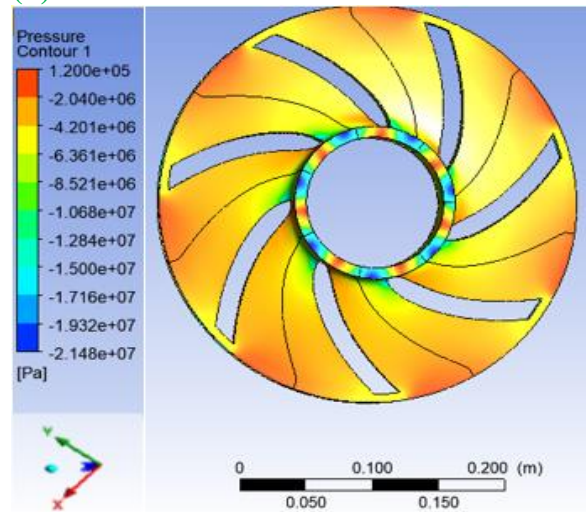
III. Methanol

Figure 3. Pressure Distribution Across the Respective Corrosive Fluids' Inlet and Outlet Angles of (a) 35 & 47° and (b) 38 & 50°

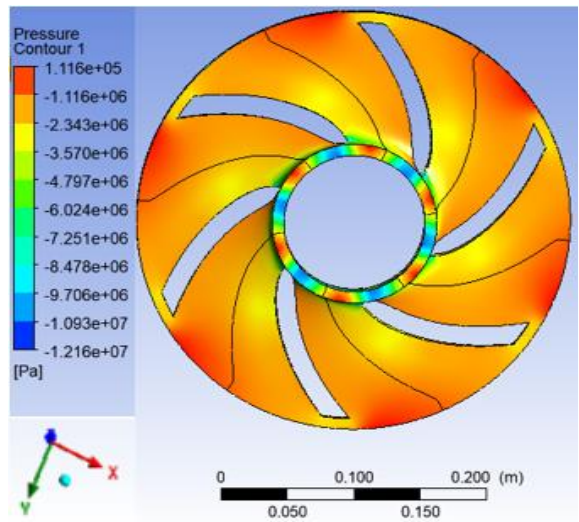
(a) Angle 35° and 47°



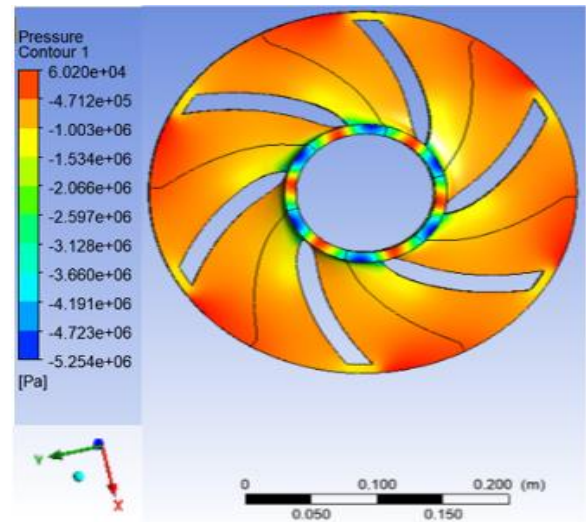
(b) 38° and 50°



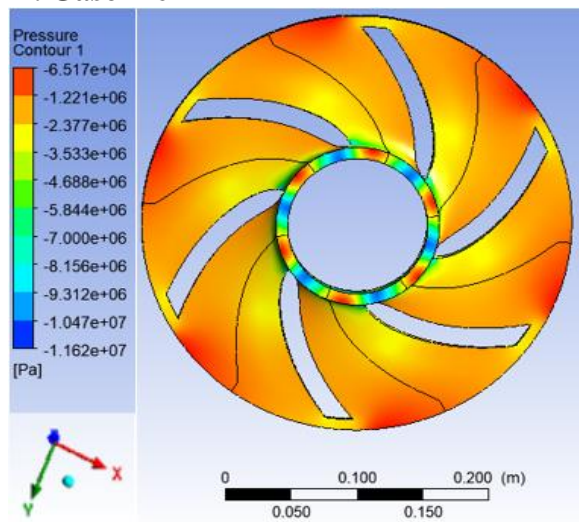
I. Water at 100°C



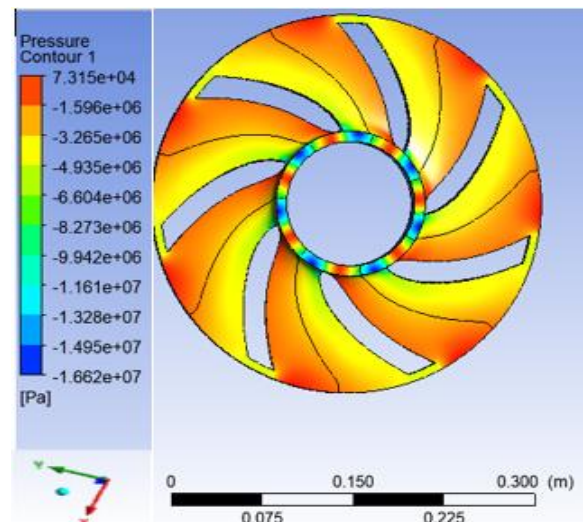
I. Water at 100°C



II. Gasoline



II. Gasoline



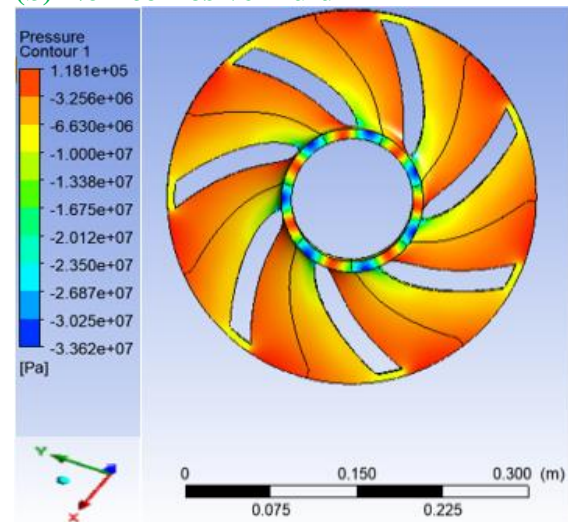
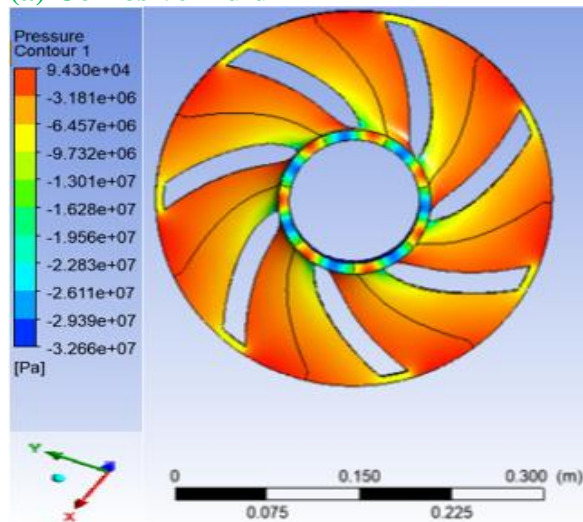
III. Kerosene

III. Kerosene

Figure 4. Pressure Distribution Across the Respective Non-Corrosive Fluids' Inlet and Outlet Angles of (a) 35 & 47° and (b) 38 & 50°

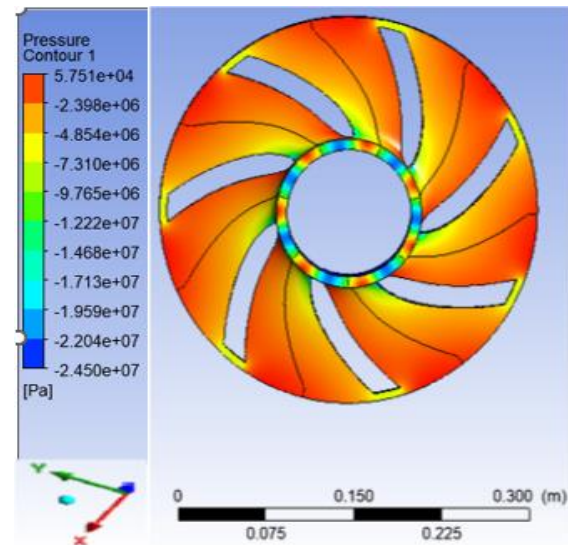
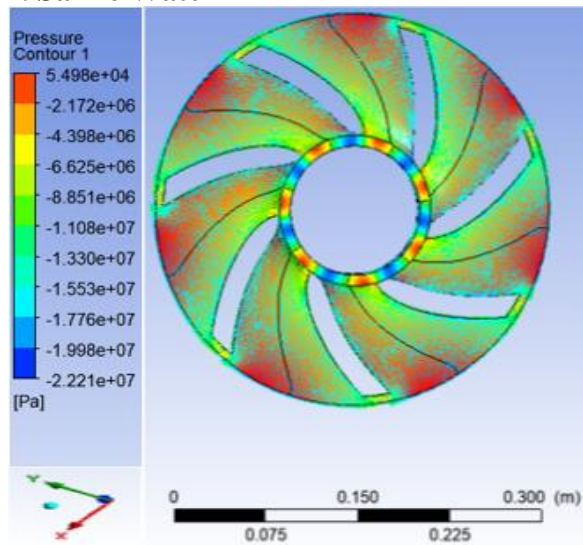
(a) Corrosive Fluid

(b) Non-corrosive Fluid



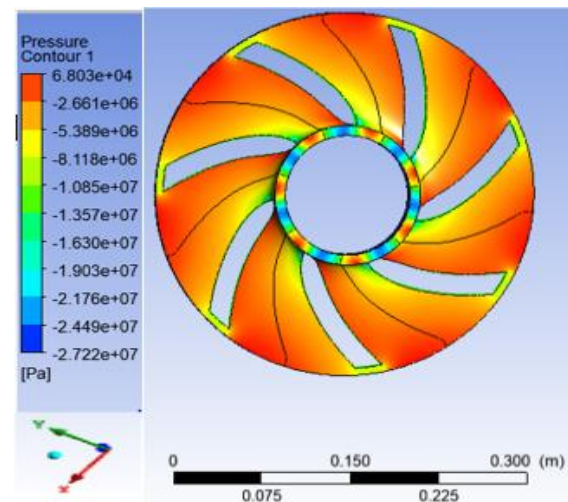
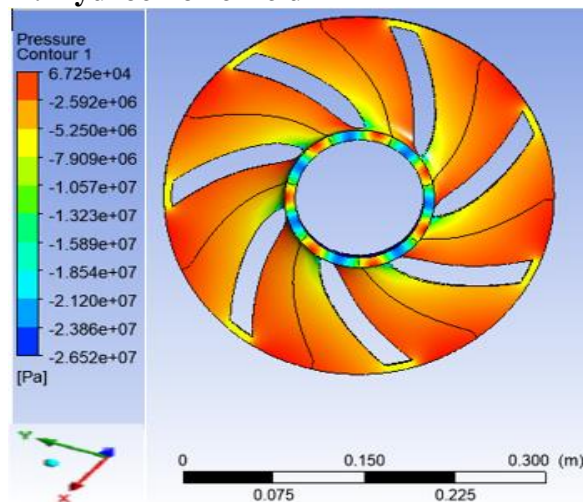
I. Saline Water

I. Water at 100°C



II. Hydrochloric Acid

II. Gasoline



III. Methanol

III. Kerosene

Figure 5: Pressure Distribution Across the Impeller Inlet Angle of 41° and Exit Angle of 53° for (a) Corrosive and (b) Non-corrosive Fluids

In Figure 4a, pressure distribution across the impeller inlet angle of 35° and exit angle of 47° for various non-corrosive fluids (water, gasoline and kerosene) have inlet pressure of -3318kPa , -1216kPa & -1421kPa and outlet pressure of 106kPa , 112kPa & 213kPa respectively. While in Figure 4b, pressure distribution across the impeller inlet angle of 38° and exit angle of 50° for water, gasoline and kerosene have inlet pressure of -2148kPa , -5254kPa & -1662kPa and outlet pressure of 60kPa , 73kPa & 118kPa respectively. The saline water, hydrochloric acid and methanol corrosive fluids have inlet pressure of -33180kPa , -988kPa & -896kPa and outlet pressure of 106kPa , 541kPa & 665kPa respectively, as shown in Figure 5a. It could also be seen from Figure 5b that pressure distribution across the impeller inlet angle of 41° and exit angle of 53° for water, gasoline and kerosene have inlet pressures of -3362kPa , -2450kPa & -2722kPa and outlet pressure of 118kPa , 58kPa & 68kPa respectively.

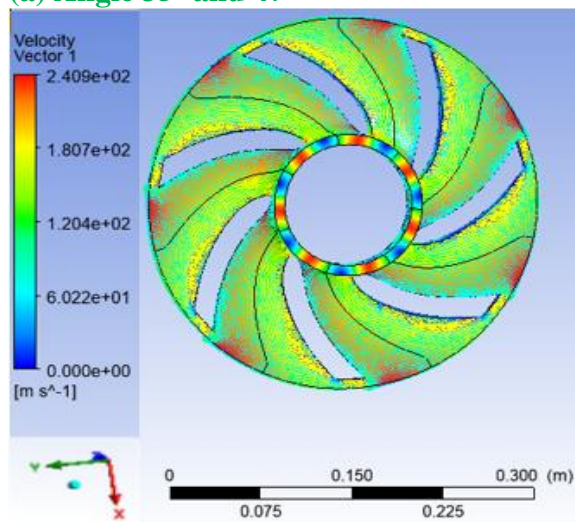
As obtained previously analyzed using ANSYS-CFX by Ding et al. (2019) and in accordance with this study, contours of static pressure and liquid flow velocity ($Q = 144 \text{ m}^3/\text{h}$) for designed impeller for corrosive and non-corrosive fluids shows that pressure and velocities were higher for non-corrosive fluids compared to corrosive fluids. The static pressure difference between impeller inlet and outlet increases with large exit blade angle. This happens because of fluid flow velocity at impeller outlet, which decreases with increase in discharge angle. The contours depicted a smooth flow as the pressure increases continuously towards the exit of the domain. So, lowest static pressure was observed at the impeller inlet on suction side.

It is clear that the pressure steadily rises from the impeller's input to its output, suggesting that the pressure there has a high gradient and the smallest value. It was observed that, at the same position, the pressure on the pressure surface is greater than the pressure on the suction surface. As a result, the back surface of the inlet is where cavitation is most likely to occur. The pressure of the tongue part will fluctuate in specific ways because of the blockage effect. By comparing the pressure distributions in Figures 3, 4, and 5, it can be deduced that the impeller's inlet pressure initially decreases and then increases, and that the change trend of the pressure distribution is consistent for various corrosive and non-corrosive fluids and different inlet and outlet angles. Keep in mind that when the flow rate is low, the pressure close to the tongue will rise when the blade outlet angle is increased.

3.2.3. Relative Velocity Distributions

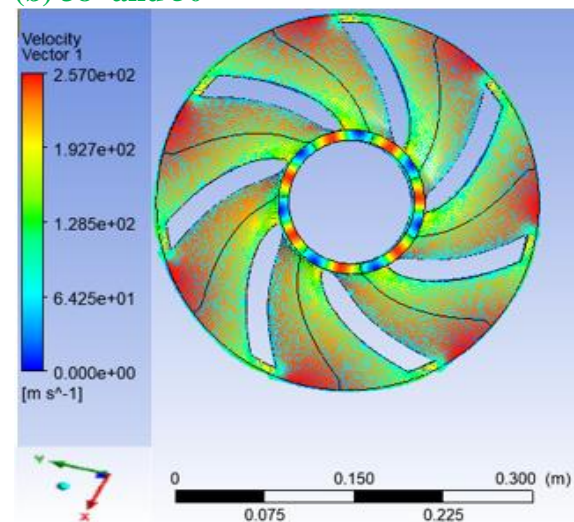
Similarly, Figures 6, 7 and 8 illustrates the velocity distributions of the impeller across the specified angles for all fluid types at the midspan of the impeller.

(a) Angle 35° and 47°

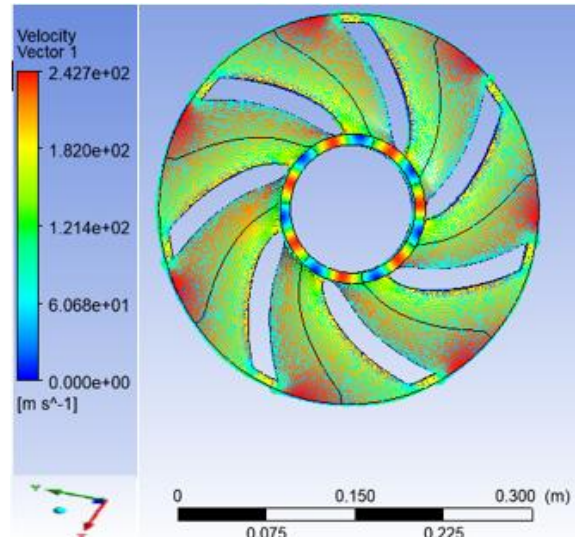
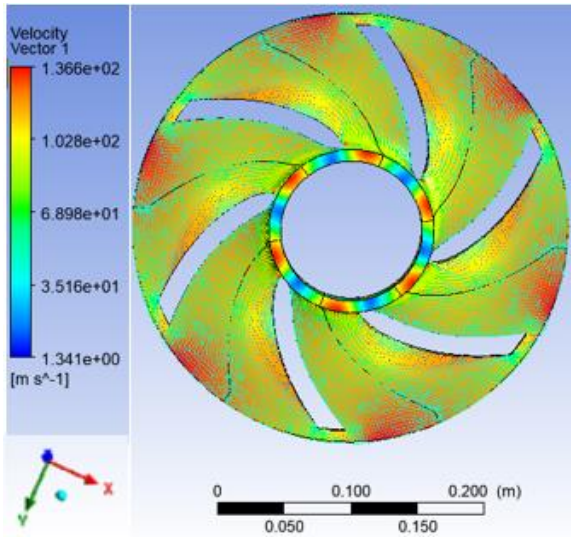


I. Saline Water

(b) 38° and 50°

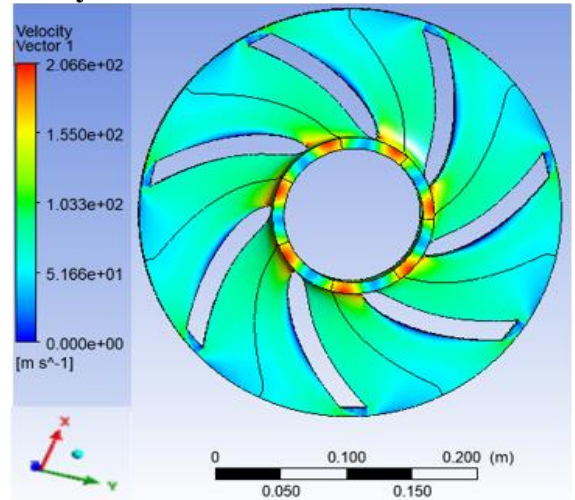
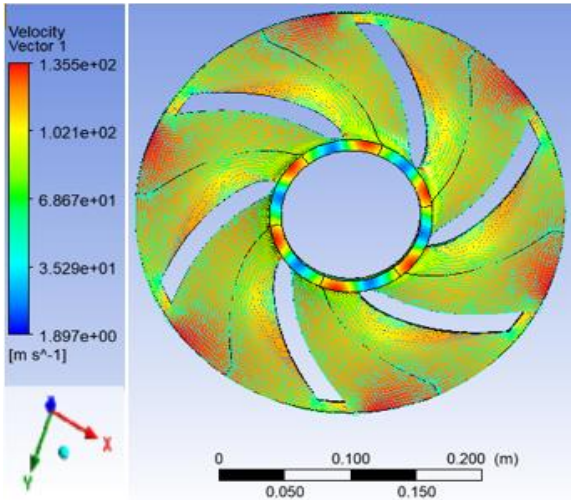


I. Saline Water



II. Hydrochloric Acid

II. Hydrochloric Acid



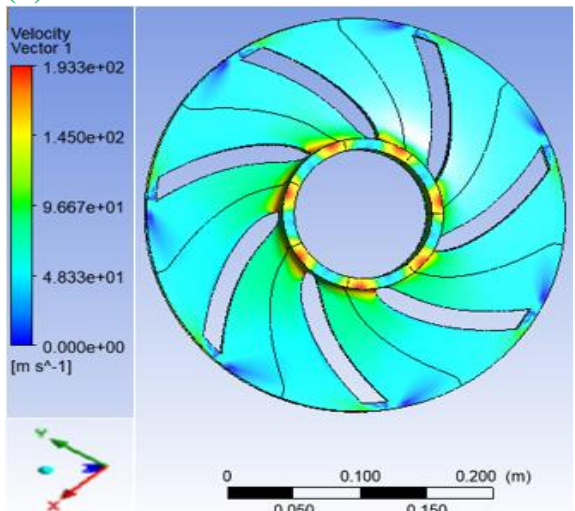
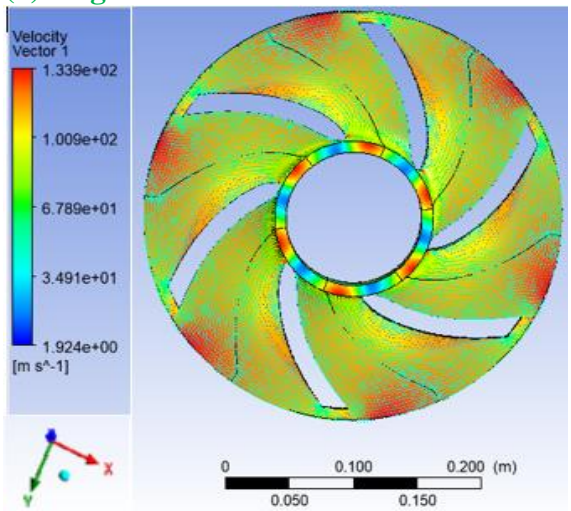
III. Methanol

III. Methanol

Figure 6. Relative Velocity Distribution at Midspan of the Respective Corrosive Fluid of the Impeller' Inlet and Outlet Angles of (a) 35 & 47° and (b) 38 & 50°

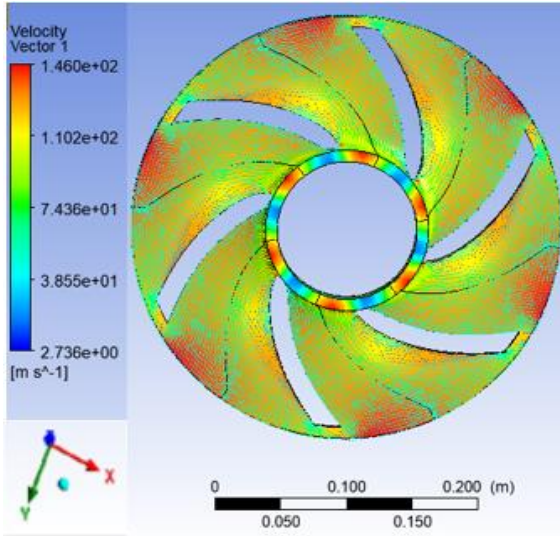
(a) Angle 35° and 47°

(b) 38° and 50°

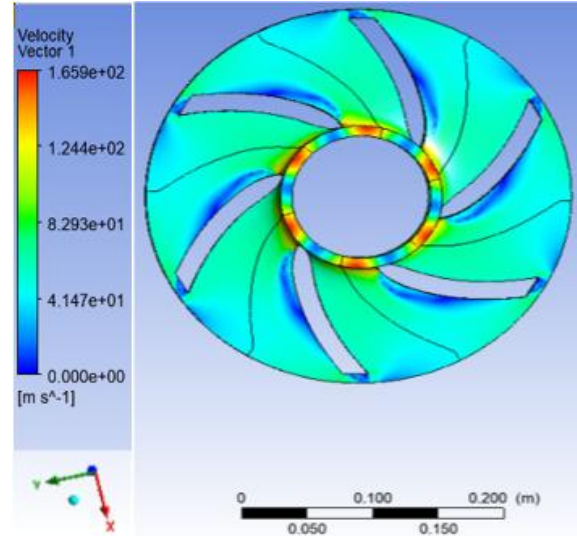


I. Water at 100°C

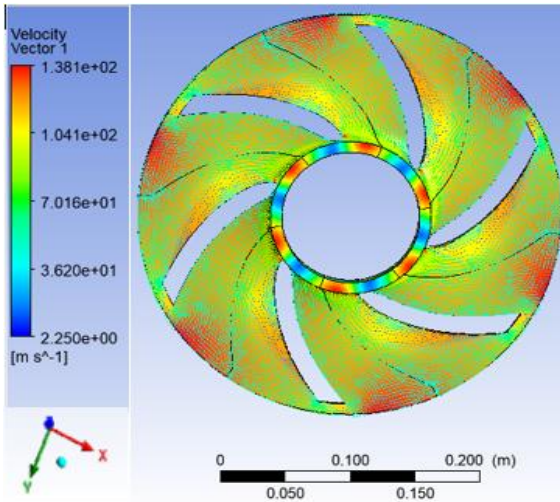
I. Water at 100°C



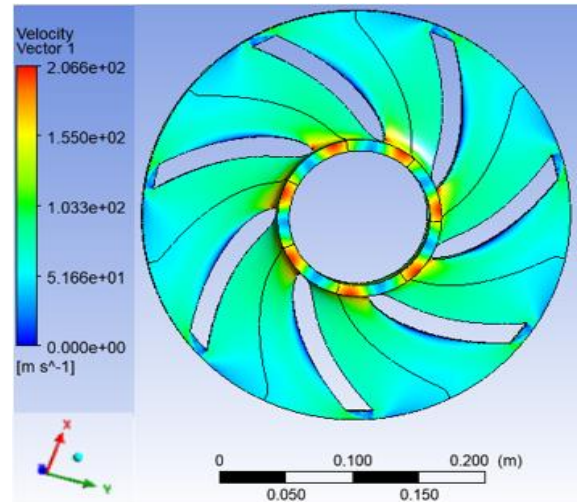
II. Gasoline



II. Gasoline



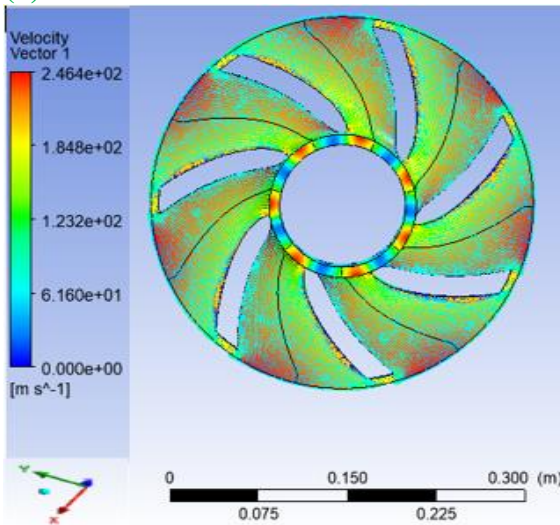
III. Kerosene



III. Kerosene

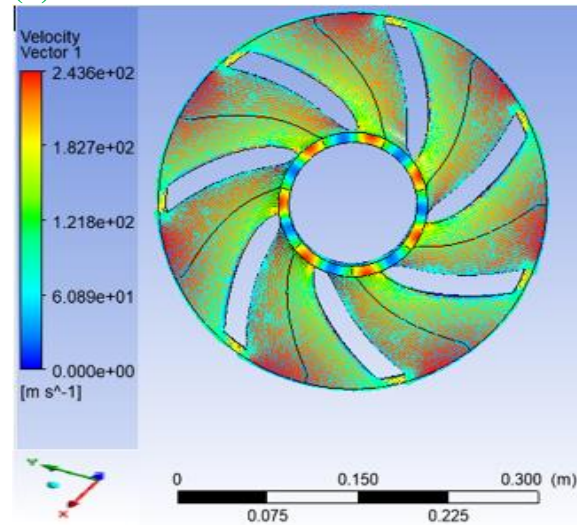
Figure 7. Relative Velocity Distribution at Midspan of the Respective Non-Corrosive Fluid of the Impeller' Inlet and Outlet Angles of (a) 35 & 47° and (b) 38 & 50°

(a) Corrosive Fluid



I. Saline Water

(b) Non-corrosive Fluid



I. Water at 100°C

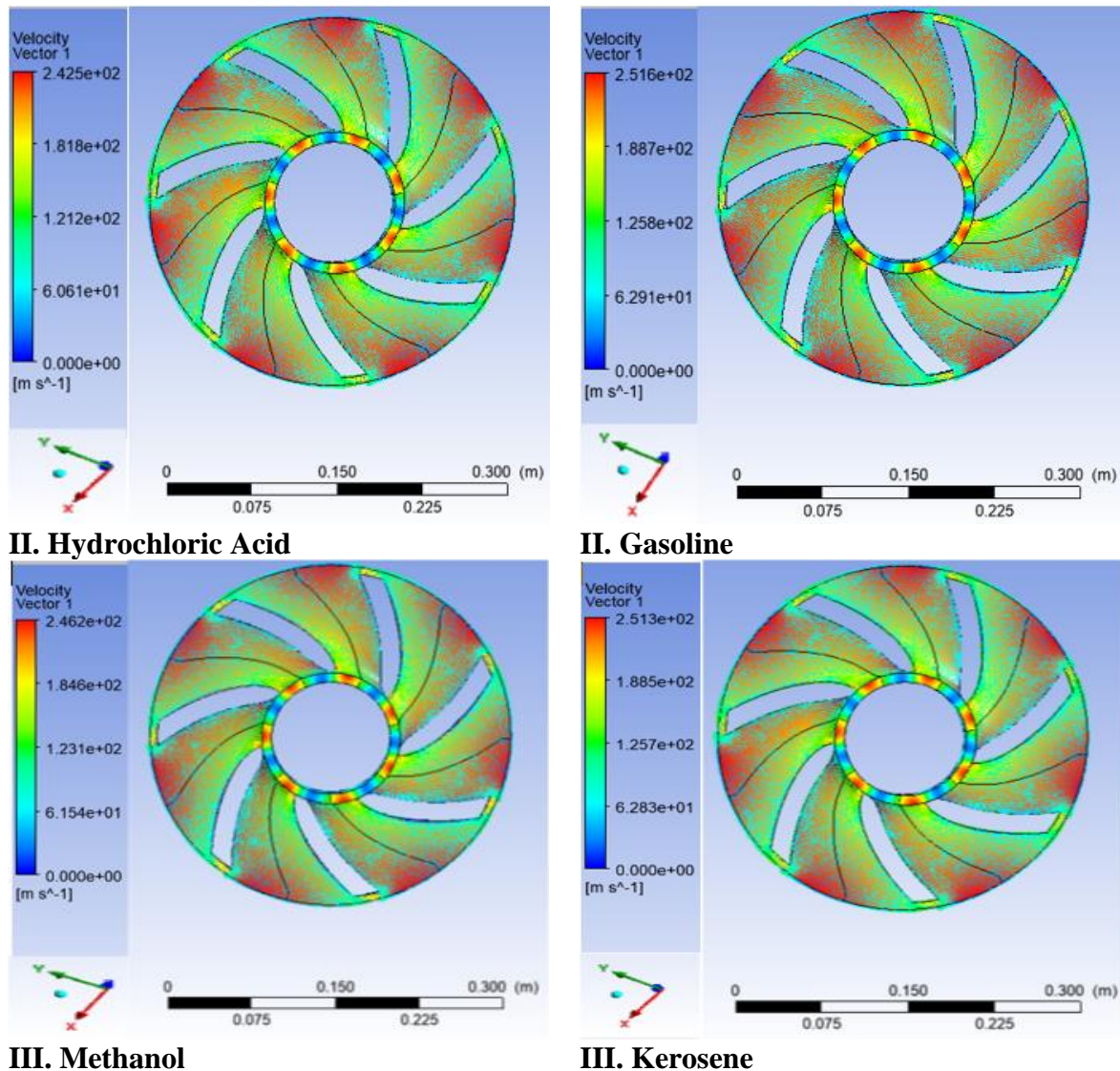


Figure 8. Relative Velocity Distribution at Midspan of the Impeller Inlet Angle of 41° and Exit Angle of 53° for (a) Corrosive and (b) Non-corrosive Fluids

Figure 6a shows the relative velocity distributions at midspan of the impeller inlet angle of 35° and exit angle of 47° for various corrosive fluids; namely, saline water, hydrochloric acid and methanol which have velocity at the impeller inlet of 0.00m/s , 1.34m/s & 1.9m/s and outlet velocity of 241m/s , 137m/s & 136m/s respectively. Also, in Figure 6b, the relative velocity distribution of the impeller inlet angle of 38° and exit angle of 50° for saline water, hydrochloric acid and methanol have velocity at the impeller inlet of 0m/s and outlet velocity of 257m/s , 243m/s & 207m/s respectively.

For non-corrosive fluids (water, gasoline and kerosene) in Figure 7a of blade inlet angle of 35° and exit blade angle of 47° , has an inlet velocity of 1.9m/s , 2.7m/s & 2.3m/s from suction side and exit velocity of 134m/s , 146m/s & 138m/s respectively. As for inlet blade angle of 41° and outlet blade angle of 53° shown in Figure 8a, the inlet velocity for various fluids is 0m/s and outlet velocity of 246m/s , 243m/s & 246m/s respectively. And as depicted in Figure 7b and Figure 8b, the relative velocity distribution across the impeller inlet angle of 38° & 41° and exit blade angle of 50° & 53° respectively for water, gasoline and kerosene fluids have inlet velocity of 0m/s and exit velocities of 193m/s , 166m/s & 207m/s and 244m/s , 252m/s & 251m/s respectively.

As can be observed, the fluid's relative velocity increases within the impeller gradually, reaching its lowest value and a lower gradient in a uniform flow at the entrance. Since the velocity at the pressure surface is greater than that on the back, the impeller outlet flow becomes unstable over time as the blade outlet angle

risers. The relative velocity was low at the impeller's input. The relative velocity reached its maximum at the impeller's exit, which was consistent with the findings of both the experimental and theoretical studies. In comparison to suction pressure, relative velocity in the pressure surface was substantially lower, also in accordance with Ding et al. (2019).

3.2.4. Performance Results of the Impeller

Table 4 shows the performance results of the impeller for corrosive and non-corrosive fluids at different impeller inlet and exit angles.

Table 4: Power (kW) for Each Impeller

Angles		Corrosive Fluids			Non-Corrosive Fluids		
Inlet	Outlet	Saline water	Hydrochloric Acid	Methanol	Water	Gasoline	Kerosene
Power (kW)							
35°	47°	659.40	478.80	582.90	194.10	367.00	596.83
38°	50°	576.20	377.53	335.64	427.20	301.22	585.40
41°	53°	549.90	343.50	396.33	505.79	322.76	420.74

Efficiency of each impeller with respect to angles and fluid type is as shown in Table 5.

Table 5: Efficiency (%) of Each Impeller

Angles		Corrosive Fluids			Non-Corrosive Fluids		
Inlet	Outlet	Saline water	Hydrochloric Acid	Methanol	Water	Gasoline	Kerosene
Efficiency (%)							
35°	47°	70.76	67.55	68.88	76.23	73.12	47.83
38°	50°	77.45	78.23	80.23	89.07	76.58	62.44
41°	53°	82.33	80.55	81.23	94.21	83.32	76.58

The performance curve for corrosive and non-corrosive fluids at different inlet and outlet angles of the impeller is shown in Figure 9.

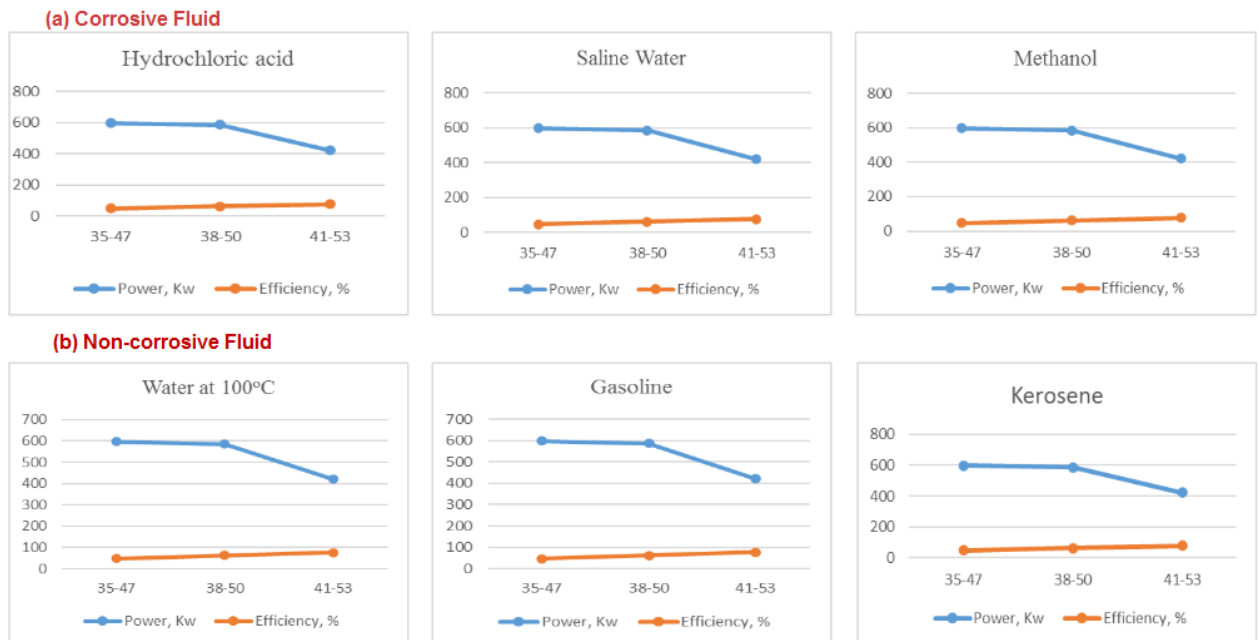


Figure 9. Performance Curves for Various (a) Corrosive and (b) Non-corrosive Fluids

It is obvious (see Figure 9a) that for saline water, shaft power of the impeller angle of 35°–47° corresponds with an increase in efficiency, while for the impeller of 38°–50° inlet and outlet angle, the power is seen to be reducing, thereby by rising the efficiency gradually. And for the impeller of 41°–53°, the shaft power

decrease continuously whereas the efficiency attained maximum. Therefore, hydrochloric acid yields the same results as that of saline water even though hydrochloric acid has maximum efficiency.

The performance curve for various non-corrosive fluids at different inlet and outlet angles of the impeller is shown in Figure 9b. Figure 9b is illustrative of the fact that for water at 100°C, at a certain shaft power of the impeller angle of 35°-47°, the efficiency increases. While for the impeller of 38°-50° inlet and outlet angle, the power is reduced, hence the efficiency gradually increases. Lastly, for impeller of 41°-53°, the shaft power continues to decrease while the efficiency attained maximum. Therefore, gasoline and kerosene also yielded the same results as that of water at 100°C which has maximum efficiency. This proved the fact that the higher the efficiency, the less energy required to operate for a specific performance point. It is clear that, as the outlet blade angle rises, the performance curve becomes flatter, same way as observed in Bacharoudis et al. (2008) who used 20°, 30° and 50° as outlet angles.

Efficiency of the impeller was calculated based on both shaft powers which operates at 2000 rpm and different mass flowrates for both corrosive and non-corrosive fluids. For the same flow rate and discharge angle, the input power is more for denser fluids. Normally, increase in flow rate results in increase in power consumption. The density of water, gasoline and kerosene is lesser than that of saline water, methanol and hydrochloric acid, which results in low power consumption. The higher the inlet and exit angles, the higher the power consumption by the impeller in accordance with Elyamin et al. (2019). A large exit angle favors efficiency improvement. This fact is also observed by Yadav & Gahlot (2015), where for an inlet angle of 20.08° and outlet angle of 16.28°, the efficiency of the pump obtained was 83%; but is 88% for an optimized angle of 20.16° and 16.62° inlet and outlet angles respectively. But when it comes to the inlet blade angle, the efficiency and H of a plastic centrifugal pump showed a decreasing trend. Thus, when selecting the best pump for application, impeller efficiency is of more paramount factor to be considered. Other variables like hub contours, impeller inlet and outlet width, shape of impeller blades, blade angle profile, viscous fluids, rotational speed, head rise and discharge rate can be optimized for high-efficiency centrifugal pump design.

4. CONCLUSION

Within the limitations of a discharge of 0.04 m³/s and a head rise of 50–75 m for various mass flow rates of corrosive and non-corrosive fluids, the centrifugal pump impeller was built and simulated in ANSYS CFX. According to the specifications and features, the centrifugal pump impeller acquired the appropriate components from the ANSYS software material library. Large slopes result in less pressure distribution at the intake, and pressure increases at the outlet as the blade outlet angle increases at various flow rates, which causes some fluctuations. However, from the study conducted by Li et al. (2021), this fluctuations can be reduced for a double-suction centrifugal pump. Due to the wear that corrosive fluids produce, non-corrosive materials enhanced the impeller's dependability and efficiency more than corrosive fluids did. Water, gasoline, and kerosene have lower densities than saline water, methanol, and hydrochloric acid, which results in lower power usage. The power used by the impeller increases together with the inlet and exit angles.

Even though the research covers a lot of area, a few limitations call for further thought on the design of a new impeller. To ascertain the surface roughness and its impact when employing corrosive fluids, additional research must be done on the centrifugal pump's impeller with volute. The performance test apparatus for centrifugal pumps should be devised and constructed for further study in order to validate the numerical result and analysis. The material's functionality should be determined using the same working limitations.

ACKNOWLEDGEMENTS

Part of this work has been published as Poster, thanks to Prof. Muhammad Nuru Idris of the Department of Chemical Engineering, University of Maiduguri, Nigeria in October, 2022.

REFERENCES

- [1] A. S. Prasad, B. L. Rao, A. Babji, and P. K. Babu, "Static and dynamic analysis of a centrifugal pump impeller," *Int. J. Sci. Eng. Res.*, vol. 4, no. 10, pp. 966–971, 2013, [Online]. Available: <http://www.ijser.org>.
- [2] Q. Zhang, H. Zhou, Q. Gao, and Z. Cui, "Analysis of effects of impeller inlet width on the performance of centrifugal pump," *J. Chem. Pharm. Res.*, vol. 6, no. 5, pp. 2078–2081, 2014, [Online]. Available: www.jocpr.com.

- [3] J. Chen, W. Shi, and D. Zhang, "Influence of blade inlet angle on the performance of a single blade centrifugal pump," *Eng. Appl. Comput. Fluid Mech.*, vol. 15, no. 1, pp. 462–475, 2021, doi: 10.1080/19942060.2020.1868341.
- [4] X. Han, Y. Kang, D. Li, and W. Zhao, "Impeller optimized design of the centrifugal pump: A numerical and experimental investigation," *Energies*, vol. 11, no. 1444, pp. 1–21, 2018, doi: 10.3390/en11061444.
- [5] K. K. Yadav and V. K. Gahlot, "Performance improvement of mixed flow pump impeller through CFD analysis," *Int. J. Res. Eng. Technol.*, vol. 4, no. 7, pp. 243–247, 2015, [Online]. Available: <http://www.ijret.org>.
- [6] S. Susilo and A. Setiawan, "Analysis of the number and angle of the impeller blade to the performance of centrifugal pump," *EUREKA Phys. Eng.*, vol. 5, pp. 53–61, 2021, doi: 10.21303/2461-4262.2021.002001.
- [7] E. C. Bacharoudis, A. E. Filios, M. D. Mentzos, and D. P. Margaris, "Parametric study of a centrifugal pump impeller by varying the outlet blade angle," *Open Mech. Eng. J.*, vol. 2, pp. 75–83, 2008.
- [8] H. Ding, Z. Li, X. Gong, and M. Li, "The influence of blade outlet angle on the performance of centrifugal pump with high specific speed," *Vacuum*, vol. 159, pp. 239–246, 2019, doi: 10.1016/j.vacuum.2018.10.049.
- [9] A. A. Adeniyi and O. D. Komolafe, "Performance analysis of an experimental centrifugal pump," *Niger. J. Technol.*, vol. 22, no. 2, pp. 149–155, 2014, doi: 10.4314/njt.v33i2.2.
- [10] S. N. Shukla and J. T. Kshirsagar, "Numerical experiments on a centrifugal pump," in *Proceedings Sciences: Fluids Engineering Division Summer Meeting*, 2009, pp. 709–719, doi: 10.1115/FEDSM2002-31176.
- [11] N. Mohamed *et al.*, "Stress analysis of various designs of centrifugal pump impellers using finite element method," *J. Eng. Technol. Adv.*, vol. 7, no. 1, pp. 36–46, 2022, doi: 10.35934/seg.v7i1.48.
- [12] M. Ashri, S. Karuppanan, S. Patil, and I. Idris, "Modal analysis of a centrifugal pump impeller using finite element method," in *MATEC Web of Conferences*, 2014, vol. 13, no. 04030, pp. 1–5, doi: 10.1051/mateconf/20141304030.
- [13] S. Rajendran and K. Purushothaman, "Analysis of a centrifugal pump impeller using ANSYS-CFX," *Int. J. Eng. Res. Technol.*, vol. 1, no. 3, pp. 1–6, 2012, [Online]. Available: www.ijert.org.
- [14] R. S. Muttali, S. Agrawal, and H. Warudhkar, "CFD simulation of centrifugal pump impeller using ANSYS-CFX," *Int. J. Innov. Res. Sci. Eng. Technol.*, vol. 3, no. 8, pp. 15553–15561, 2014, doi: 10.15680/IJRSET.2014.0308066.
- [15] G. R. H. A. Elyamin, M. A. Bassily, K. Y. Khalil, and M. S. Gomaa, "Effect of impeller blades number on the performance of a centrifugal pump," *Alexandria Eng. J.*, vol. 58, pp. 39–48, 2019, doi: 10.1016/j.aej.2019.02.004.
- [16] M. N. Idris and I. U. Usman, "Design studies using corrosive and non-corrosive materials to improve on reliability and efficiency of an impeller of a centrifugal pump," in *The Electrochemical Society (ECS) Meeting Abstracts, Volume MA2022-02 Z01: General Student Poster Session*, 2022, vol. MA2022-02, no. 64, pp. 2345–2345, doi: 10.1149/MA2022-02642345mtgabs.
- [17] I. U. Usman and M. N. Idris, "Experimental studies and designs using corrosive and non-corrosive materials to improve on reliability and efficiency of an impeller of a centrifugal pump," in *CHE 599 Proposal Presentation 2021/2022 Session*, 2021, pp. 1–1, [Online]. Available: <https://www.researchgate.net/publication/356894529>.
- [18] M. Murakami, K. Kikuyama, and E. Asakura, "Velocity and pressure distributions in the impeller passages of centrifugal pumps," in *Symposium on Measurement Methods in Rotating Components of Turbomachinery, Gas Turbine and Fluids Engineering Conference, New Orleans, La*, 1980, vol. 102, pp. 420–420, [Online]. Available: <https://fluidsengineering.asmedigitalcollection.asme.org>.
- [19] X. Jia, B. Cui, Z. Zhu, and X. Yu, "Numerical investigation of pressure distribution in a low specific centrifugal pump," *J. Therm. Sci.*, vol. 27, pp. 25–33, 2018, doi: 10.1007/s11630-018-0980-9.
- [20] Q. Li, S. Li, P. Wu, B. Wuang, and D. Wu, "Investigation on reduction of pressure fluctuation for a double-suction centrifugal pump," *Chinese J. Mech. Eng.*, vol. 34, no. 12, pp. 1–18, 2021, doi: 10.1186/s10033-020-00505-8.